Snap-back repellers and chaotic attractors

Laura Gardini*
Department of Economics and Quantitative Methods, University of Urbino, Urbino, Italy

Fabio Tramontana†
Department of Economics, University of Ancona, Ancona, Italy and Department of Economics and Quantitative Methods, University of Urbino, Urbino, Italy

(Received 1 February 2010; revised manuscript received 27 February 2010; published 7 April 2010)

When homoclinic orbits to an expanding periodic point exist, the point is called a snap-back repeller. Here, we consider the two-dimensional piecewise-linear map in canonical form, continuous and discontinuous, showing how snap-back repellers may be associated with robust chaotic attracting sets (not only with chaotic repellers). Examples are given both for the continuous and discontinuous maps.

DOI: 10.1103/PhysRevE.81.046202 PACS number(s): 05.45.−a

I. INTRODUCTION

Since the pioneering work of Poincaré, in the last 60 years the studies on homoclinic orbits were mainly associated with saddle cycles in flows [1,2]. As well as the transverse homoclinic and heteroclinic points of saddle cycles, homoclinic orbits and chaotic dynamics associated with saddle-foci cycles have also been studied (see [3,4] and the surveys books [5,6]). Dealing with orbits homoclinic to saddles or saddle foci, the common factor is that homoclinic orbits can be studied in suitable *invertible* maps. Thus, homoclinic orbits to expanding repelling points (when all the eigenvalues are higher than 1 in modulus) cannot occur.

However, recent applications in physics and engineering have lead to noninvertible piecewise smooth systems. Several works have been published dealing with the two-dimensional piecewise-linear map in canonical form, where the parameters are the determinants and the traces of two linear maps f_L and f_R which are defined in two half planes L and R,

$$f:(x,y)\mapsto\begin{cases}f_L(x,y), & (x,y)\in L\\ f_R(x,y), & (x,y)\in R,\end{cases} \tag{1}$$

where

$$f_L:\begin{pmatrix}x\\y\end{pmatrix}\mapsto\begin{pmatrix}\tau_L x+y+\mu_L\\-\delta_L x\end{pmatrix},\quad L=\{(x,y):x\le 0\}, \tag{2}$$

$$f_R:\begin{pmatrix}x\\y\end{pmatrix}\mapsto\begin{pmatrix}\tau_R x+y+\mu_R\\-\delta_R x\end{pmatrix},\quad R=\{(x,y):x>0\}. \tag{3}$$

Here, τ_L,τ_R are the traces and δ_L,δ_R are the determinants of the Jacobian matrix of the map f in the left and right half planes, i.e., in L and R, respectively, $\mathbb{R}^2=L\cup R$. The map is continuous when $\mu_L=\mu_R$ and discontinuous otherwise.

This model was introduced as a generalization of the one-dimensional piecewise-linear skew-tent map by Nusse and Yorke [7]. Since then, it has been investigated in many papers (see [8–18] to cite a few) and is often used in applications [19–23].

For a wide region of the parameter space, the map (1) is noninvertible. In fact, assuming both determinants δ_L and δ_R different from zero, when they have opposite sign, $\delta_L\delta_R<0$, then Eq. (1) is noninvertible. We remark that the case in which one determinant is equal to zero is particular because a half plane is mapped into the critical line $y=0$, so it is indeed noninvertible. It is degenerate, however, since the set of noninvertible points is only the critical line (a set of zero measure in the phase space) and the preimage of one critical point is a half line. When $\delta_L\delta_R<0$, however, the region of points having two distinct rank-one preimages is a half plane. In this case, there exists a new type of homoclinic orbit associated with repelling nodes and foci which, as recalled above, cannot occur in invertible systems. Marotto was the first to prove in [24] that homoclinic orbits may occur also for these repelling points and that chaos is associated with the existence of homoclinic orbits, introducing the term of snap-back repellers (SBRs). Indeed, his first work included a minor technical mistake and he himself gave a corrected version in [25] after the appearance of several papers which, trying to correct the mistake, provided less general proofs (as in Li and Chen [26]).

Recently, the same map (1) has been considered in [27], showing how SBR also can occur in that standard map. All the examples shown there, however, are associated with "chaotic repellers." That is, the chaotic sets associated with SBR nodes exist on invariant sets of zero measure in the phase space and almost all the trajectories are divergent. It is clear that this situation is not useful in the applications. Moreover, it is a widely shared opinion that SBRs are associated with this kind of "repelling chaos." Maybe this is quite common when repelling nodes are considered, while this is not generically true when repelling foci become SBR. In fact, as we shall see in this work, when a repelling focus is surrounded by an annular invariant chaotic area, then it is highly probable that the SBR bifurcation leads to a chaotic

*laura.gardini@uniurb.it
†f.tramontana@univpm.it

attractor.[1] This property was first evidenced in [28] (see also in [29]). Recently, in [30], the Marotto's results were also generalized to continuous and discontinuous piecewise smooth systems.

The purpose of the present work is to show how common are the snap-back repellers in the piecewise-linear canonical map (1) both in the continuous case ($\mu_L=\mu_R$, considered in Sec. II) and in the discontinuous one ($\mu_L\neq\mu_R$, considered in Sec. III), leading to robust (in the sense of [19], as persistent as a function of the parameters) chaotic attractors. Moreover, we shall also see the occurrence of the first homoclinic bifurcation, that is, the transition of a repelling cycle to SBR, showing that it is associated with critical homoclinic orbits. In fact, in the cases of repelling foci here described, in which the cycles are surrounded by an annular chaotic area, the transition to SBR occurs when the first-rank preimage of the cycle, from outside the area, merges on the boundary and the boundary consists of critical segments. Section IV concludes.

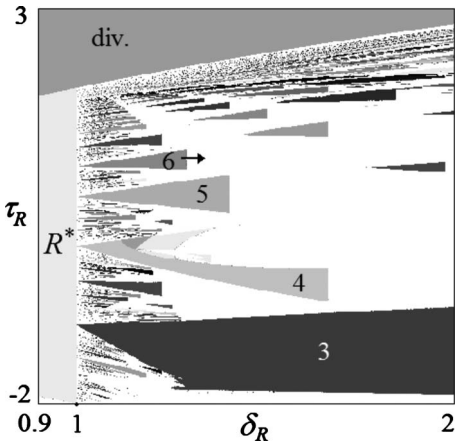

FIG. 1. Two-dimensional bifurcation diagram in the parameter plane (δ_R,τ_R) at $\tau_L=0.3$, $\delta_L=-0.6$ fixed. White points denote chaos or cycles of period greater than 45.

II. CONTINUOUS CASE

Following [30], the border line $x=0$ is denoted LC_{-1} and its forward images by using f_L and f_R are called *critical lines*. Let L^* and R^* denote the fixed points of f_L and f_R determined by

$$\left(\frac{\mu_i}{1-\tau_i+\delta_i},\frac{-\delta_i\mu_i}{1-\tau_i+\delta_i}\right),\quad i=L,R,$$

respectively. L^* is the fixed point of the map f if $\mu_L/(1-\tau_L+\delta_L)\leq 0$, otherwise it is a so-called virtual fixed point. Similarly, R^* is the fixed point of f if $\mu_R/(1-\tau_R+\delta_R)\geq 0$, otherwise it is virtual. The stability of the fixed point R^* is defined by the eigenvalues $\lambda_{1,2(R)}$ of the Jacobian matrix of the map f_R, which are

$$\lambda_{1,2(R)}=(\tau_R\pm\sqrt{\tau_R^2-4\delta_R})/2. \tag{4}$$

Let us consider here the following parameters: $\tau_L=0.3$, $\delta_L=-0.6$, at which L^* is virtual, while we need R^* to exist as an unstable focus in the continuous case with $\mu_L=\mu_R=1$.

The two-dimensional bifurcation diagram in Fig. 1 shows in different gray tonalities periodicity regions associated with cycles of different periods appearing after the *center bifurcation*, Neimark-Sacker bifurcation for piecewise-linear maps of the fixed point R^*, occurring at $\delta_R=1$. The term *center bifurcation* is used in this case (see [14]) because the bifurcation associated with complex eigenvalues in a linear map is of this kind. At the bifurcation value (here $\delta_R=1$), the fixed point R^* is a center and when the rotation number associated with the complex eigenvalues is rational, there exists an invariant polygon filled with periodic orbits, while an invariant ellipse filled with quasiperiodic orbits exists when the rotation number is irrational. In [14], the boundary of this invariant region is completely characterized, as well as the closed invariant curve which is the resulting attracting set after the bifurcation, for $\delta_R>1$.

As we can see from the structure of the bifurcation curves in Fig. 1, in infinitely many periodicity regions, the attracting cycle leads to a secondary center bifurcation as the cycle becomes a repelling focus. This will allow us to show first the snap-back bifurcation of a cycle and then that of the fixed point R^*, all leading to chaotic attractors. As an example, we have taken the parameters δ_R and τ_R inside the region of the attracting six-cycle, but it is clear that similar results can be observed taking the parameters inside other periodicity regions. As long as a point (δ_R,τ_R) is inside the periodicity region of the six-cycle (the analog of an Arnold's tongue), the attracting six-cycle existing after the center bifurcation of the fixed point is an attracting node, coupled with a saddle six-cycle, and the unstable set of the saddle gives a saddle-node connection which represents a closed invariant attracting curve (also called torus connection). The destruction of this closed invariant curve can occur in several different ways and has been studied in several papers. In the periodicity regions shown in Fig. 1, this torus destruction occurs due to the transition of the eigenvalues from real to complex, so that the six-cycle attracting node becomes a six-cycle attracting focus. The vertical border observed in the periodicity region of the cycle corresponds to the transition six-cycle attracting focus to six-cycle repelling focus. That is, a *secondary center bifurcation* occurs: the six fixed points of the piecewise-linear map f^6 have the same kind of bifurcation as the one described above for the fixed point. When the parameters are taken exactly on the vertical boundary, six closed invariant polygons or six closed invariant elliptic regions exist (depending on the rotation number), which are followed by six closed invariant attracting curves. Increasing the parameter δ_R, these closed curves are destroyed and sequences of homoclinic bifurcations of some saddle cycles lead to six cyclical annular chaotic regions as shown in Fig. 2(a).

In Fig. 2(a), we can see that the fixed point R^* is far from the chaotic areas and that the six cyclical chaotic areas have an annular structure. Notice that the numerical simulation in Fig. 2(a) clearly shows the existence of annular areas around

[1]Although this is not necessarily always true because the transition "chaotic attractor to chaotic repeller" may occur "before" the SBR bifurcation, in which case the SBR bifurcations are not associated with the existence of a chaotic attractor.

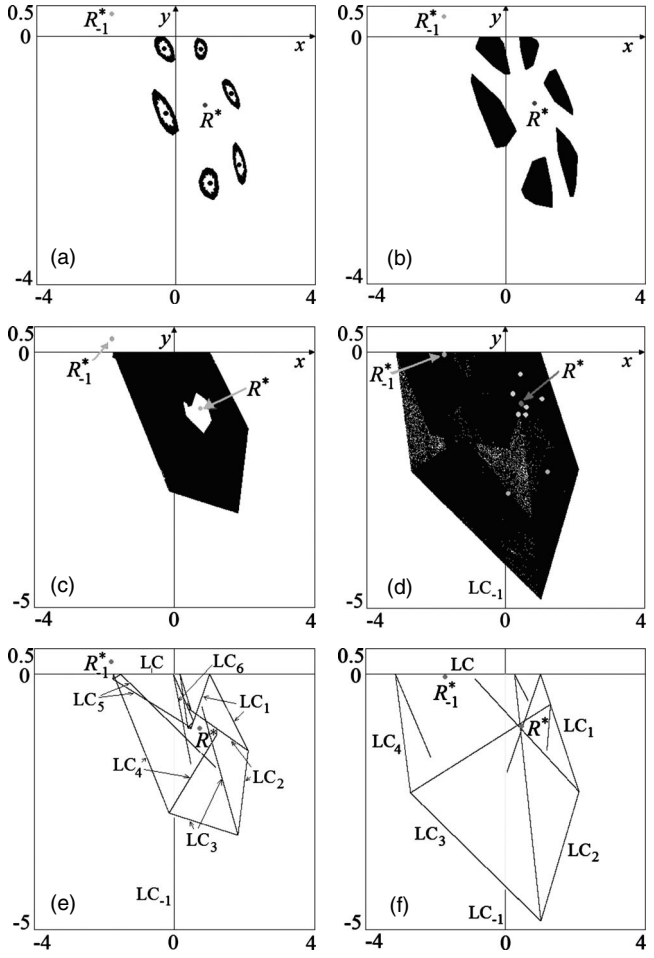

FIG. 2. Attracting sets at $\tau_L=0.3$, $\delta_L=-0.6$, $\mu_L=\mu_R=1$, and $\tau_R=1.1$. (a) $\delta_R=1.3$; (b) $\delta_R=1.35$; (c) $\delta_R=1.5$; (d) $\delta_R=2.3$. (e) Boundary of the annular chaotic area shown in (c). (f) Boundary of the chaotic area shown in (d).

the cycle and even if we do not prove rigorously the existence of true robust chaos, the relevant fact is that the cycle cannot have homoclinic orbits. In fact, as long as the six areas have a hole inside, then the six-cycle repelling focus is not a SBR: no homoclinic orbits to it can exist. The six-cycle becomes a SBR when the holes disappear, leading to six closed chaotic regions, as shown in Fig. 2(b). Continuing to increase the parameter δ_R, the six pieces merge into a unique annular chaotic area [Fig. 2(c)] but as long as there is a hole around the fixed point R^*, the fixed point cannot be a SBR because there are no homoclinic orbits to it. In fact, the simply connected region D given by the annular area and the hole inside [see Fig. 2(c)] is invariant, $f(D)=D$, and the rank-one preimage of R^* distinct from itself, that is, $R^*_{-1}=f_L^{-1}(R^*)$, given by

$$f_L^{-1}(R^*)=\left(\frac{\delta_R\mu_R}{\delta_L(1-\tau_R+\delta_R)},\frac{\delta_L\mu_R-\tau_L\delta_R\mu_R}{\delta_L(1-\tau_R+\delta_R)}-\mu_L\right), \quad (5)$$

is external to this area [see Fig. 2(c)] and thus external to D are necessarily also all its further preimages (although here, there are no further preimages).

However, even in cases in which the rank-one preimage R^*_{-1} is below the line $y=0$ external to the invariant area D, all the other preimages are necessarily outside the invariant area. This is simple to prove (as shown also in [28,30]): if not, assume that a preimage of some rank k is in D, then after k iterations this point must be still in D, while after k iterations, it is mapped in R^*_{-1} external to D, which is a contradiction. Inside the invariant area D, the trajectory of a point inside the hole, different from the fixed point, spirals and enters the chaotic annular set. Thus, no point of this invariant area can be mapped close to the fixed point unstable focus, so that it cannot have homoclinic trajectories. This can be stated as follows: as long as the rank-one preimage of the fixed point R^* different from itself, say $R^*_{-1}=f_L^{-1}(R^*)$, is external to the invariant area, the fixed point cannot be a SBR. Increasing the parameter δ_R, the hole around R^* decreases and the transition to SBR occurs when the preimage R^*_{-1} contacts the boundary of the chaotic area, crossing the boundary made up of critical curves and entering inside the chaotic area, together with R^*. In Fig. 2(d), we also show a few preimages of R^*_{-1} with the inverse f_R^{-1},

$$f_R^{-1}(u,v)=(-v/\delta_R,u-\mu_R+\tau_R v/\delta_R),$$

which reaches R^* showing that this is a homoclinic orbit and that R^* is now a SBR.

We note that in the works by Marotto, as well as in [27], nothing is stated about the bifurcation which leads a repelling fixed point from not a SBR (i.e., without homoclinic orbits) to a SBR (i.e., to have homoclinic orbits). As we have seen above, in the case of a cycle repelling focus for which an invariant annular area exists bounded by critical curves, this bifurcation can be precisely studied. Let us first recall that the boundary of the chaotic area is given by arcs of critical curves obtained iterating the so-called "germ" on LC_{-1}, which is given by the portion of critical curve $x=0$ inside the invariant area. This is proved in [30], however, we can easily recall here this property. Given an invariant set A, which means that $f(A)=A$, let $(g)=A\cap LC_{-1}=A\cap(x=0)$. Then the image $f(A)$ includes $f(g)$ which belongs to LC (the line $y=0$) on the external boundary. As the set A is invariant, all the forward images of (g) belong to A, and as $f(g)$ is on the external boundary, all its images are either on the boundary or inside. In particular, all the boundary points are necessarily belonging to segments images of portions of (g). In Fig. 2(e), we show that both the internal and external boundaries of the annular chaotic set are obtained by seven images of the small generating segment (g) on $x=0$ given by $y\in[-2.8,0]$. As the parameter δ_R increases, the preimage R^*_{-1} comes closer to LC $(y=0)$ and the hole around the fixed point R^* shrinks to the point itself. At the bifurcation value $\delta_R=2.2$, at which R^*_{-1} belongs to the boundary $y=0$ of the chaotic area, the hole has disappeared and the fixed point R^* is crossed by all the critical lines of any rank. This is the homoclinic bifurcation, or SBR bifurcation, leading a repelling focus to become SBR and is associated with infinitely many critical homoclinic orbits (critical because all the homoclinic orbits must have a point on the critical set $x=0$). After the contact, when R^* and R^*_{-1} are inside [as shown in Fig. 2(f), where the boundary of the invariant area is ob-

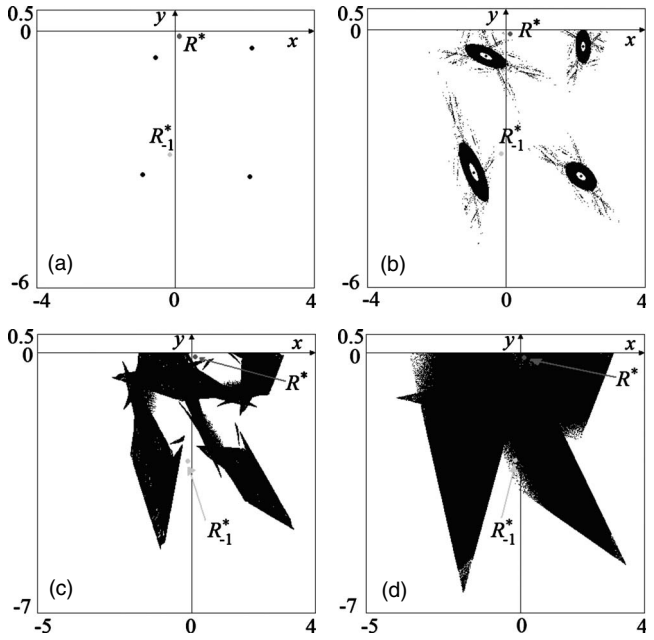

FIG. 3. Attracting sets at $\tau_L=0.3$, $\delta_L=-0.6$, $\mu_L=3$, $\mu_R=0.1$, and $\tau_R=1.1$. (a) $\delta_R=1.53$; (b) $\delta_R=1.5385$; (c) $\delta_R=1.6$; (d) $\delta_R=1.9$.

tained by five images of the generating segment (g) on $x=0$ given by $y\in[-4.2,0]]$, there is an explosion of infinitely many noncritical homoclinic orbits [one of which is shown in Fig. 2(d)].

It is now clear that a similar bifurcation occurs for the six-cycle: considering the power f^6 of the map, each point is a fixed point of a piecewise-linear map, with suitable critical curves, and the annular chaotic regions are bounded by segments of critical curves. The SBR bifurcation commented above occurs when the rank-one preimage of the cycle merges on the boundary of the annular area.

III. DISCONTINUOUS CASE

A behavior similar to the one described in the previous section occurs also in the discontinuous case. Let us fix the following parameters, $\tau_L=0.3$, $\delta_L=-0.65$, at which L^* is virtual, in the discontinuous case with $\mu_L=3$ and $\mu_R=0.1$. At $\tau_L=1.1$ and $\delta_R=1.53$, the fixed point R^* is an unstable focus and a stable four-cycle around it exists, as shown in Fig. 3(a). Then, as before, increasing the parameter δ_R, we can see the secondary center bifurcation of the four-cycle followed by chaotic areas [Fig. 3(b)]. After that, we have first the transition to SBR of the four-cycle [as we can see, no holes exist in Fig. 3(c)] while the fixed point R^* and its rank-one preimage $R^*_{-1}=f_L^{-1}(R^*)$ are far from the one-piece chaotic area. Increasing the parameter δ_R, in Fig. 3(d) we can see that these two points are inside the chaotic area and homoclinic orbits to R^* can be found. As before, the fixed point R^* becomes a SBR when its rank-one preimage R^*_{-1} has a contact with the chaotic area, entering inside it. We only note that the difference with respect to the continuous case is in the arcs of critical curves bounding the invariant areas. In the continuous case, the critical set LC is a curve: it is the unique

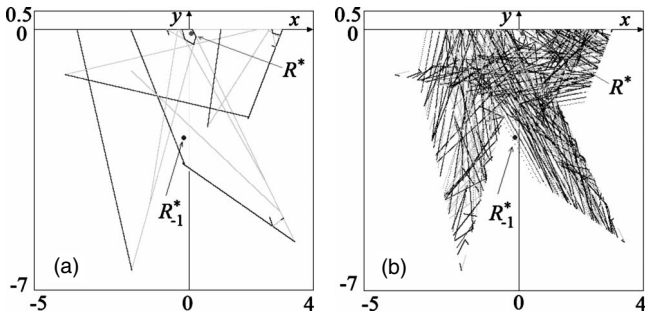

FIG. 4. Images of critical segments.

image of $x=0$ and the boundary of an invariant area is obtained by the images of a unique arc of critical curve. While in the discontinuous case we have two critical curves LC obtained by the images of $x=0$ with the two functions f_L and f_R. The boundaries of an invariant area are detected by taking the images of an arc of $x=0$ both with f_L and f_R.

In Fig. 4(a), we show the boundary of the invariant area in the case of Fig. 3(d), which is obtained by six iterations of the generating segment (g) on $x=0$ given by $y\in[-3.8,0]$. The iterations $f_R^k(g)$ are shown in black, those of $f_L^k(g)$ in gray. In Fig. 4(b), we show 35 images of a very small segment on $x=0$ (given by $y\in[-0.2,0]$) close to the fixed point R^*, showing that we can reach the point R^*_{-1}, thus giving numerical evidence of the existence of preimages of R^*_{-1} reaching the fixed point R^* and giving homoclinic orbits, so that it is a SBR.

We remark that the continuous and discontinuous cases are not so much different. As noticed above, the difference with respect to the continuous case is only in the arcs of critical curves bounding the invariant areas. Thus, having a fixed point in the right side R, the important fact is that the preimage of the fixed point crosses the boundary through a critical arc belonging to the images $f_R^k(g)$ which indeed occurs in our example, as shown Fig. 4(a), where these critical arcs are in black. In both cases (continuous and discontinuous), we have that before the first SBR bifurcation, no homoclinic orbit can exist. The first SBR bifurcation occurs when the rank-one preimage of the fixed point (or cycle) under study merges with a critical segment on the boundary of the annular absorbing area. In both cases at the bifurcation value, we have infinitely many homoclinic orbits and all are critical. On the other side, after the bifurcation, in both cases we have an explosion of noncritical homoclinic orbits (this is the reason why such bifurcations are also called Ω explosions).

IV. CONCLUSIONS

In this work, we have shown how common snap-back repellers are in the piecewise-linear canonical map (1), particularly when associated with repelling cycles which are foci. In such cases, we have shown that the transition of a cycle from repelling focus to SBR often leads to attracting chaotic areas, both in the continuous ($\mu_L=\mu_R$) and in the discontinuous ($\mu_L\neq\mu_R$) maps. That is, the snap-back repeller may be trapped inside an invariant chaotic attractor,

which is robust, as persistent as a function of the parameters. Moreover, we have shown how it is possible to characterize the first transition of a cycle to SBR via the occurrence of critical homoclinic orbits. The existence of an annular chaotic area leads to a quite easy condition characterizing the bifurcation value leading to the first SBR. However, it is worth noticing that this first bifurcation is generally followed by other "homoclinic explosions" leading to an increase of the homoclinic orbits and always characterized by the occurrence of critical homoclinic orbits. As one-dimensional analog, we can consider the first SBR bifurcation occurring to the positive fixed point in the well-known logistic map $x' = \mu x(1-x)$, which is then followed by infinitely many other homoclinic explosions as the parameter μ tends to 4.

[1] S. Wiggins, *Global Bifurcations and Chaos* (Springer-Verlag, New York, 1988).

[2] S. Wiggins, *Introduction to Applied Nonlinear Dynamical Systems and Chaos* (Springer-Verlag, New York, 2003).

[3] L. P. Shilnikov, Math. USSR Sb. **10**, 91 (1970).

[4] L. P. Shilnikov, Int. J. Bifurcat. Chaos Appl. Sci. Eng. **7**, 1953 (1997).

[5] L. P. Shilnikov, A. L. Shilnikov, D. Turaev, and L. Chua, *Methods of Qualitative Theory in Nonlinear Dynamics. Part 1*, World Scientific Series on Nonlinear Science, Series A Vol. 4 (World Scientific, Singapore, 1998).

[6] L. P. Shilnikov, A. L. Shilnikov, D. Turaev, and L. Chua, *Methods of Qualitative Theory in Nonlinear Dynamics. Part 2*, World Scientific Series on Nonlinear Science, Series A Vol. 5. (World Scientific, Singapore, 2001).

[7] H. E. Nusse and J. A. Yorke, Physica D **57**, 39 (1992).

[8] S. Banerjee and C. Grebogi, Phys. Rev. E **59**, 4052 (1999).

[9] S. Banerjee, P. Ranjan, and C. Grebogi, IEEE Trans. Circuits Syst., I: Fundam. Theory Appl. **47**, 633 (2000).

[10] M. Dutta, H. E. Nusse, E. Ott, J. A. Yorke, and G. H. Yuan, Phys. Rev. Lett. **83**, 4281 (1999).

[11] L. Gardini, V. Avrutin, and M. Schanz, Grazer Mathematische Berichte **354**, 53 (2009).

[12] M. A. Hassouneh, E. H. Abed, and H. E. Nusse, Phys. Rev. Lett. **92**, 070201 (2004).

[13] D. J. W. Simpson and J. D. Meiss, SIAM J. Appl. Dyn. Syst. **7**, 795 (2008).

[14] I. Sushko and L. Gardini, Int. J. Bifurcat. Chaos Appl. Sci. Eng. **18**, 1029 (2008).

[15] I. Sushko and L. Gardini, Int. J. Bifurcat. Chaos Appl. Sci. Eng. (to be published).

[16] Z. T. Zhusubaliyev, E. Mosekilde, S. Maity, S. Mohanan, and S. Banerjee, Chaos **16**, 023122 (2006).

[17] Z. T. Zhusubaliyev, E. Mosekilde, S. De, and S. Banerjee, Phys. Rev. E **77**, 026206 (2008).

[18] Z. T. Zhusubaliyev, E. Mosekilde, and S. Banerjee, Int. J. Bifurcat. Chaos Appl. Sci. Eng. **18**, 1775 (2008).

[19] S. Banerjee, J. A. Yorke, and C. Grebogi, Phys. Rev. Lett. **80**, 3049 (1998).

[20] M. Di Bernardo, M. I. Feigen, S. J. Hogan, and M. E. Homer, Chaos, Solitons Fractals **10**, 1881 (1999).

[21] Y. Guohui, S. Banerjee, E. Ott, and J. A. Yorke, IEEE Trans. Circuits Syst., I: Fundam. Theory Appl. **45**, 707 (1998).

[22] Y. Ma, M. Agarwal, and S. Banerjee, Phys. Lett. A **354**, 281 (2006).

[23] S. Parui and S. Banerjee, Chaos **12**, 1054 (2002).

[24] F. R. Marotto, J. Math. Anal. Appl. **63**, 199 (1978).

[25] F. R. Marotto, Chaos, Solitons Fractals **25**, 25 (2005).

[26] C. Li and G. Chen, Chaos, Solitons Fractals **18**, 69 (2003); **20**, 655E (2004).

[27] P. Glendinning and C. H. Wong, Phys. Rev. E **79**, 025202(R) (2009).

[28] L. Gardini, Nonlinear Anal. Theory, Methods Appl. **23**, 1039 (1994).

[29] C. Mira, L. Gardini, A. Barugola, and J. C. Cathala, *Chaotic Dynamics in Two-Dimensional Noninvertible Maps* (World Scientific, Singapore, 1996).

[30] L. Gardini and F. Tramontana, Regular Chaotic Dyn. (to be published).